Vibrational Coherence Spectroscopy Identifies Ultrafast Branching in an Iron(II) Sensitizer

F. Hainer, N. Alagna, A. Reddy Marri, T. Penfold, Philippe Gros, S. Haacke, T. Buckup

Vibrational Coherence Spectroscopy Identifies Ultrafast Branching in an Iron(II) Sensitizer

F. Hainer[1,2], N. Alagna[1,2], A. Reddy Marri[4], T. J. Penfold[5], P.C. Gros[4], S. Haacke*[3], T. Buckup*[1,2]

[1]Physikalisch Chemisches Institut, Ruprecht-Karls Universität, D-69120 Heidelberg, Germany

[2]Centre for Advanced Materials, Ruprecht-Karls Universität, D-69120 Heidelberg, Germany

[3]University of Strasbourg – CNRS, IPCMS, Strasbourg, France

[4]Université de Lorraine, CNRS, L2CM, F-54000 Nancy, France

[5]Chemistry-School of Nat. & Env. Sci., Newcastle University, Newcastle Upon-Tyne, UK

*Corresponding Authors:

tiago.buckup@pci.uni-heidelberg.de, Phone: +49 (0)6221 54 8723, Fax: +49 (0)6221 54 8730

stefan.haacke@ipcms.unistra.fr, Phone: +33(0)388107171; Fax: +33(0)388107145

Abstract

The introduction of N-heterocyclic carbene ligands has greatly increased the lifetimes of metal-to-ligand charge transfer states (MLCT) in iron(II) complexes, making them promising candidates for photo-catalytic applications. However, the spectrally elusive triplet metal-centered state (^{3}MC) has been suggested to play a decisive role in the relaxation of the MLCT manifold to the ground state, shortening their lifetimes and consequently limiting the application potential. In this work, time-resolved vibrational spectroscopy and quantum chemical calculations are applied to shed light on the ^{3}MCs involvement in the deactivation of the MLCT manifold of an iron(II) sensitizer. Two distinct symmetric Fe-L breathing vibrations at frequencies below 150 cm^{-1} are assigned to the ^{3}MC and ^{3}MLCT by quantum chemical calculations. Based on this assignment, an ultrafast branching directly after excitation forms not only the long lived ^{3}MLCT but also the ^{3}MC as an additional loss channel.

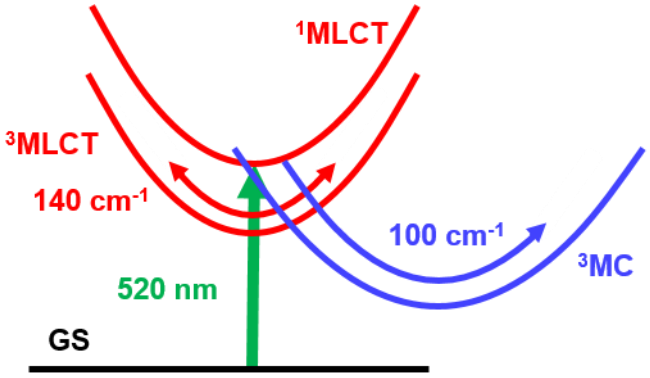

Over the past ten years, research on metal-organic complexes based on first row transition metals - Fe, Cu, Cr or Zr - has witnessed an increasing attention, driven by the ambitious aim of conferring these materials with interesting photophysical properties such as strong absorption over a broad spectral range and high fluorescence/ luminescence quantum yields through sufficiently long excited state lifetimes (ESL).[1-4] The obvious target is to tune their properties making them functionally relevant for light-induced applications.[5] The main challenge is to replace scarce and thus expensive noble metals such as Ru, Ir or Pt, which are the gold standards in the area of metal-organic complexes designed for the above applications. Iron, the lighter homolog of Ru, is the most earth-abundant metal and thus has been particularly scrutinized. However, due to the primogenic effect, its small ligand field splitting energy (LFSE) is a severe drawback.[6, 7] A breakthrough came from the recent pioneering work of K. Wärnmark's group, reporting on Fe coordinated with four strong σ-donating N-heterocyclic carbene (NHC) ligands to form the complex $[Fe(bmip)_2]^{2+}$, where bmip = 2,6-bis(3-methyl-imidazole-1-ylidine)-pyridine. This Fe(II) complex affords a sufficiently large increase of the LFSE to prevent the ultrafast excited state relaxation into the counterproductive low energy metal-centered quintet ^{5}MC[8-11]. Most remarkably, the lifetime of the metal-to-ligand-charge transfer triplet (^{3}MLCT) was enhanced 100-fold compared to $[Fe(bpy)_3]^{2+}$, allowing for efficient electron injection into TiO_2 photoanodes,[12] and solar cell operation was demonstrated, with the COOH-substituted derivative $[Fe(bmipc)_2]^{2+}$.[5] This triggered the development of different classes of Fe(II) and Fe(III) compounds with very promising properties in terms of applications,[5, 13-15] provided the extended nanosecond excited state lifetimes are indeed due to MLCT or LMCT states only.[16] However, some recent reports pointed out that the excited state lifetime is

determined by specific reaction coordinates, and that an ultrafast branching can create a superposition of ^{3}MLCT and non-reactive ^{3}MC states.[17-20] Standard transient absorption spectroscopy (TAS) is limited in discriminating between these two kinds of states.[21] XFEL-based femtosecond X-ray emission and scattering probing the spin state of the Fe(II) gives a clearer insight, and revealed an ultrafast parallel population of ^{3}MLCT and ^{3}MC[19] but requires large scale facilities with often limited beam time. Thus, it is now highly desirable to develop a lab-based fs spectroscopy approach to identify the nature of the excited state(s), and become an analytical method for a large set of compounds.

In this work, the involvement of the spectrally elusive ^{3}MC state in the photophysics of $[Fe(bmipc)_2]^{2+}$ is addressed. This compound is a promising sensitizer for solar energy conversion previously studied by TAS.[22] The identified sequential $^1MLCT \rightarrow {}^3MLCT \rightarrow {}^3MC$ has, however, to be questioned, in the light of the fast branching into ^{3}MLCT and ^{3}MC identified for the parent $[Fe(bmip)_2]^{2+}$. Impulsive Vibrational Spectroscopy (IVS) and Pump-Impulsive Vibrational Spectroscopy (Pump-IVS)[23] are therefore employed, identifying a parallel population of both ^{3}MC and ^{3}MLCT states.

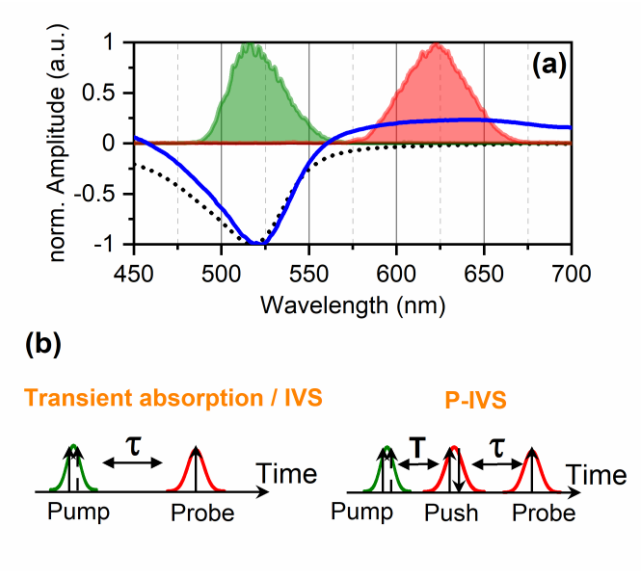

Figure 1 (a) Actinic pump (green) and push/probe spectra (red) used in the impulsive vibrational spectroscopy experiments. Transient absorption signal at T=0.2 ps (blue) and inverted ground state absorption spectra (dotted) for reference. (b) Schematic representation of the pulse sequences in the conducted experiments. T denotes the delay of the push pulse with respect to the pump pulse. τ denotes the rapid scanned probe delay with respect to the pump pulse.

In IVS, vibrational wavepackets are induced by an ultrashort pump pulse initially in the Franck-Condon (FC) region in the excited state potential surface.[23] IVS, being the impulsive analogous of transient absorption, maps how initially induced vibrational wavepackets evolve from the FC in the different relaxation pathways. Results of the IVS experiment are summarized in Figure 2 (see SI Sections 3 and 4 for full dataset). Here, the actinic pump was tuned to be resonant with the lowest ground state absorption band of $[Fe(bmipc)_2]^{2+}$ at 520 nm (Figure 1a). A selected IVS transient (650 nm) is given in Figure 2a and clearly shows modulations of several frequency contributions from a vibrational wavepacket. Fitting the non-oscillatory (population) exponential behaviour in time yields the coherent vibrational contribution as residual (Figure 2b). Low frequency oscillations with a large amplitude dominate the initial 700 fs. At longer delays, persistent higher frequency oscillations with a smaller amplitude become dominant and form a beating node at $\tau = 1.75$ ps. A

quantitative analysis of these oscillations can be obtained by fitting them as a sum of independent sine functions (see SI Section 6 for details). The results from this fit are shown in Table 1. As expected, the low-frequency oscillation (94 cm^{-1}) is assigned the largest amplitude by far and shows a very short damping time of 420 fs, which matches previously observed vibrations for the parent $[Fe(bmip)_2]^{2+}$.[19] The other two oscillations at 352 cm^{-1} and 382 cm^{-1} show lifetimes of 1.44 ps and 1.08 ps, respectively. These frequencies match the Fe-N stretch and ligand backbone deformation (350 cm^{-1}) reported for $[Fe(bmip)_2]^{2+}$ [24] and a well-known deformation vibration of acetonitrile (379 cm^{-1}), which was used as solvent. The fit also reproduces the 30 cm^{-1} (1.11 ps period) beatings between them, forming nodes at 0.6 ps and 1.70 ps. Figure 2c shows the residual of this fit.

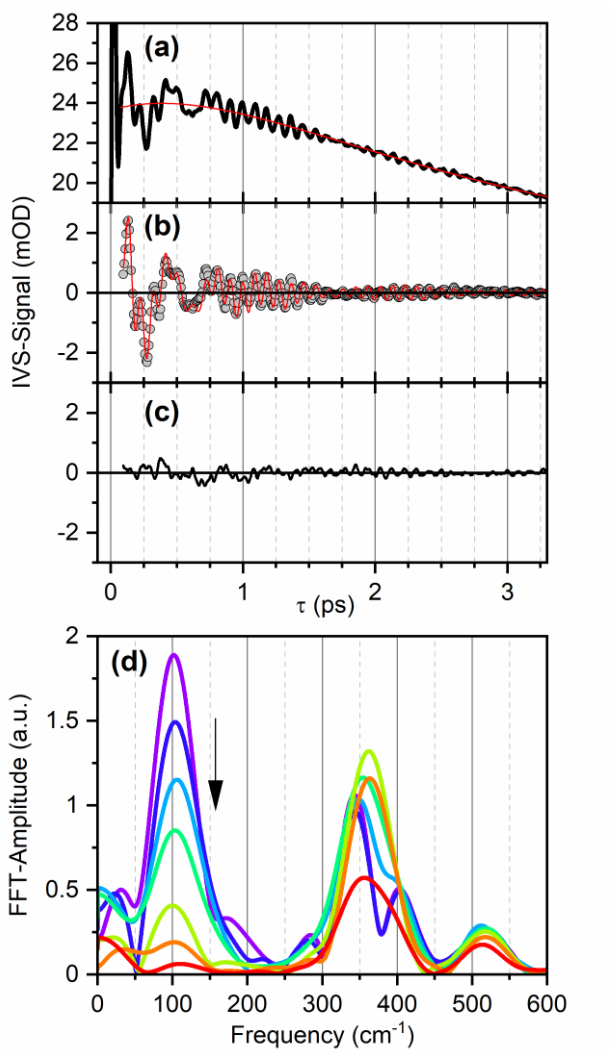

Figure 2 (a) Transient (black) obtained by IVS-experiment at 650nm and exponential fit (red) of the electronic population contribution. (b) Coherent vibrational contribution (circles) obtained as residual, as well as oscillatory fit thereof (red) including the residual (c). (d) Selected vibrational spectra obtained by sliding window Fourier transformation (1 ps trace length, 0.1 ps step size, Gaussian window). Sliding window shift (from violet to red): 0 ps, 0.1 ps, 0.2 ps, 0.3 ps, 0.5 ps, 0.7 ps, 1.0 ps.

The temporal evolution of this coherent vibrational signal has also been analysed via a sliding window fast Fourier transformation (SW-FFT, Figure 2d). In this approach, the 352 cm^{-1} and 382 cm^{-1} frequencies cannot be resolved due to their interference and the limited frequency resolution (transients constrained to 1 ps duration). This leads to the merging and separation for different SW-shifts shown in Figure 2d. The

mode at 520 cm^{-1} is in good agreement with a ligand distortion vibration identified by quantum chemical calculations (513 cm^{-1}, see SI section 7, Fig. S10).

Table 1 – Impulsive Vibrational Spectroscopy: Results from fit and FFT

Oscillatory fit (full trace)				FFT (0-1 ps)
ν (cm^{-1})	Ampl. (mOD)	τ (fs)	ϕ (rad)	ν (cm^{-1})
94	2.19	420	1.23	101
352	0.756	1440	3.26	343
382	0.546	1080	3.51	403

The lowest frequency is quantified by the SW-FFT at 101 cm^{-1} with a dephasing time around 350 fs (see marked decline in Figure 2d and SI Fig. S8), which is in good agreement with the oscillatory fitting. These results are now discussed with reference to time constants obtained from global analysis of TAS (220 fs, 5.3 ps, 19.9 ps, see SI Section 2) and literature. In accordance with the findings of Kunnus et al. for frequency and dephasing times of this low frequency mode in the parent $[Fe(bmip)_2]^{2+}$,[19] the 101 cm^{-1} mode is assigned to a coherent breathing vibration in the ^{3}MC. It is important to note, that this vibration is not induced by a Raman process within the ^{3}MC, which is not populated at the time of the pump arrival. It is instead initiated by an ultrafast population of ^{3}MC in the following way. The transition from the MLCT manifold to the ^{3}MC state comes with a significant shift in equilibrium Fe-L bond length, as has been reported for $[Fe(bmip)_2]^{2+}$ (~0.1 Å).[19, 25] If this transition occurs impulsively with respect to the 330 fs oscillation period, a wavepacket is launched on the ^{3}MC surface along this breathing mode. A similar contribution from the ^{3}MLCT is not to be expected, since the equilibrium geometries of the GS, ^{1}MLCT and ^{3}MLCT are very similar (nested oscillators, see SI Fig. S9). In this regard, the

time constant of this impulsive population of the ^{3}MC is unlikely to be the 220 fs obtained in the global analysis of the TAS signal (see SI Section 2) though. An impulsive relaxation of the MLCT manifold would require a relaxation much faster than the 330 fs oscillation period (100 cm^{-1}). It is likely that this time constant is distorted due to the overlap with oscillatory features at initial probe delays. Indeed, the ^{1}MLCT lifetime measured by up-conversion fluorescence experiments is expected to be faster than 190 fs.[26] Although the lifetime of the ^{1}MLCT cannot be precisely determined in these experiments, it is more likely that the branching is taking place at the ^{1}MLCT and not at the ^{3}MLCT state. This is justified by (i) the lack of any vibrational coherence signature typical of the ^{3}MLCT (vide infra) at early probe delays and (ii) the DADS spectrum for the 220 fs component (Fig.S3(f)). Indeed, if the branching took place in the ^{3}MLCT, one would expect the first species observed in the global analysis to be a hot vibrationally level in the ^{3}MLCT state and show a blue shift and narrowing during the relaxation. But, the DADS rather display a 220 fs rise of the ^{3}MLCT ESA (600-670 nm), and reshaping of ESA during the 5.3-ps interval (Fig. S3(f)).

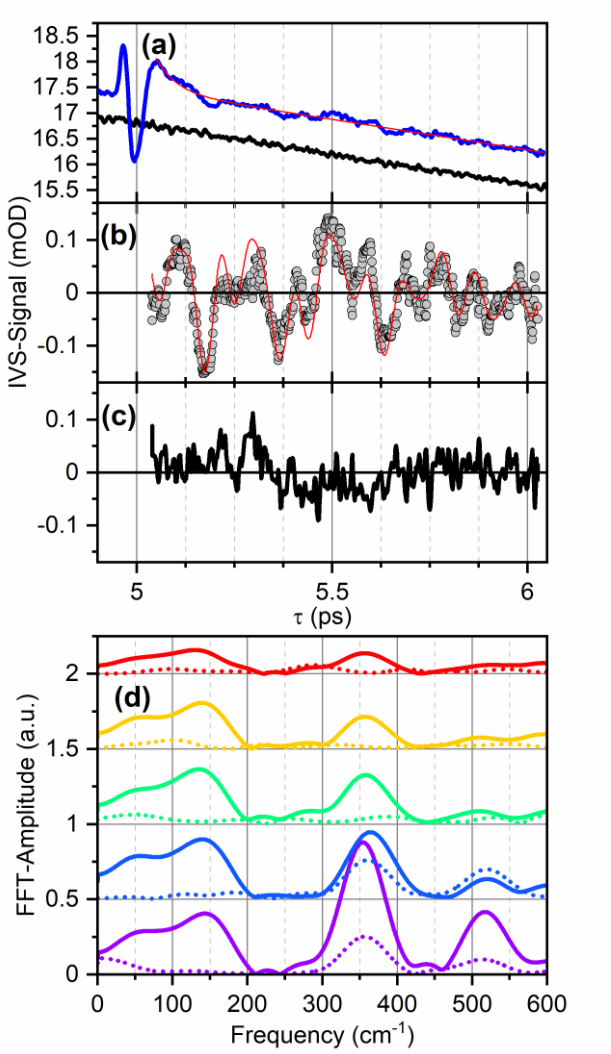

Figure 3 Exemplary transient obtained at 650 nm by Pump-IVS (T = 5 ps) (blue, vertically shifted by 0.5 OD) and IVS (black) for reference. Subtraction of biexponential fit (red) yields the oscillatory residuals (circles) in (b). Oscillatory fit (b, red) and residual thereof (c). (d) Vibrational spectra obtained by Fourier transformation of IVS (dotted), and Pump-IVS experiments (solid lines) at different (T-)delays (from violet to red): 2 ps, 3 ps, 5 ps, 10 ps, 20 ps.

With the 101 cm^{-1} vibration established as fingerprint of the ^{3}MC state, we focused our studies on the question, how this vibration evolves on the ps timescale. Since these vibrations fully dephase during the first picosecond, pump-IVS experiments were conducted with an additional pulse, called “push”-pulse, resonant exclusively with the excited state absorption at λ > 575 nm. The purpose of this push pulse is to reinduce a vibrational wavepacket at a waiting time T (Figure 1b) within the excited

state manifold. Pump-IVS contrasts to IVS in this regard, since the push pulse reinduces vibrational wavepackets even after full vibrational dephasing and, thus, maps e.g. frequencies change during the waiting time T.[23] Comparing the frequencies of the vibrational wavepackets induced near the FC region (IVS experiments) with those induced at later times (Pump-IVS), during the excited state relaxation, may give evidence for new electronic states. Figure 3a shows exemplary transients (650 nm, T=5 ps) of an experiment with (Pump-IVS) and without the push pulse (IVS). In this direct comparison it becomes apparent, that vibrational coherences are successfully reinduced, after the coherences induced by the actinic pump have dephased. The oscillatory fit as described above (see also SI section 6) of the exemplary Pump-IVS trace (Figure 3b) determines two modes in the frequency region typical for Fe-L stretch vibrations (i.e. below 200 cm^{-1}) at 117 cm^{-1} and 157 cm^{-1}. The latter shows a significantly larger amplitude and a lifetime similar to the 101 cm^{-1} mode from the IVS experiment (vide supra).

Table 2 – Pump- Impulsive Vibrational Spectroscopy: Results from fit and FFT

Oscillatory fit				FFT (T = 5 ps)
ν (cm^{-1})	Ampl. (mOD)	τ (fs)	ϕ (rad)	ν (cm^{-1})
117	0.060	1170	3.79	56
157	0.166	304	0.07	140
357	0.076	1380	2.14	357
519	0.037	650	3.23	510

Although the FFT (Figure 3d) is unable to reliably resolve the interfering frequencies below 200 cm^{-1}, a direct comparison of Pump-IVS and IVS shows the ≈ 140 cm^{-1}

mode is not present after 2 ps in IVS (Table 1), but can be reinduced via the push pulse (Fig. 3d). Most notably, these vibrations can be reinduced even 20 ps after photoexcitation by the actinic pump.

The significant blue shift from 100 cm^{-1} to 140 cm^{-1} contradicts an assignment to the Fe-L breathing mode within the ^{3}MC. This shift is, however, in good agreement with the shift obtained for normal modes calculated for ^{3}MC: ν_{18} = 148 cm^{-1} and for ^{3}MLCT: ν_{21} = 175 cm^{-1}. Importantly, the Raman activity of the mode on the ^{3}MLCT surface is about 1.8 times greater than that on the ^{3}MC state (see SI Section 7, Figure S10). This factor is actually squared in the case of the self-heterodyne detected non-linear third order signal probed by IVS and becomes >3. In addition, the temporal evolution of the reinducibility of this mode is in good agreement with the population dynamics of the ^{3}MLCT obtained from TAS (see Figure 4c). Hence, the 140 cm^{-1} mode is here assigned to a breathing vibration on the ^{3}MLCT. The 100 cm^{-1} mode of the ^{3}MC, however, is either not reinduced or dominated by the ^{3}MLCT mode as soon as 2 ps after photoexcitation.

The presence of ^{3}MC characteristic modes immediately after photoexcitation sheds light on the ^{3}MC states involvement in the photophysics of $[Fe(bmipc)_2]^{2+}$. The 100 cm^{-1} mode observed in the IVS experiment shows (vide supra), that the intersystem crossing (ISC) from the initially populated ^{1}MLCT to the long-lived ^{3}MLCT is not complete, but a fraction of the ^{1}MLCT population branches into the ^{3}MC fast enough to observe coherent breathing motions with a 100 cm^{-1} frequency. This is consistent with the sub-200fs ^{1}MLCT lifetime found by fluorescence up-conversion on the same compound.[26] The branching ratio in the parent $[Fe(bmip)_2]^{2+}$ was suggested to be dependent on the photon energy, with higher energies favouring the population of the ^{3}MC.[19] The present experiments with little to no

excess photon energy are in line with this conjecture, since no fractional GSB recovery or any other UV-VIS spectroscopic indication of the ^{3}MC is identified, as reported for $[Fe(bmip)_2]^{2+}$.[27] Therefore, the branching ratio can only be estimated to significantly favour the ^{3}MLCT over the ^{3}MC. Nevertheless, in spite of its minor population, the ^{3}MC can be clearly observed via IVS.

Finally, the lack of reinducibility of the ^{3}MC associated breathing mode in the Pump-IVs experiments at later delays is not a decisive experimental proof of a *parallel relaxation mechanism* (Figure 4a). If the ^{3}MC lifetime is much shorter than that of the long lived ^{3}MLCT ($\tau_{3MC} \ll \tau_{3MLCT}$), *a sequential decay* (Figure 4b) would result in an "inverted kinetics" scheme and explain the experimental observations as well. In this regime, the ^{3}MC population is very small after the fraction from the initial branching has returned to the ground state, i.e. at all delays > τ_{3MC}. Hence, the different population dynamics become virtually indistinguishable (Figure 4c). The assumption of a short lived ^{3}MC is supported by the absence of the characteristic mode 2 ps after photoexcitation and ^{3}MC lifetimes of 2.2 ps reported for an Iron(II)-NHC complex[28] and 1.5 ps for the parent $[Fe(bmip)_2]^{2+}$.[19] In this regard, the 5.3 ps lifetime identified by TAS is significantly too long to be assigned to the ^{3}MC. Instead, it is assigned to a vibrational cooling within the ^{3}MLCT, which is also supported by the blue shift and similarity of the corresponding decay associated difference spectra (DADS, SI Section 2, Figure S3f). With respect to the ^{3}MC lifetime, we can therefore only refer to the 420 fs dephasing time of its characteristic Fe-L stretch vibration as a lower boundary and the lack of reinducibility after 2 ps as an upper boundary.

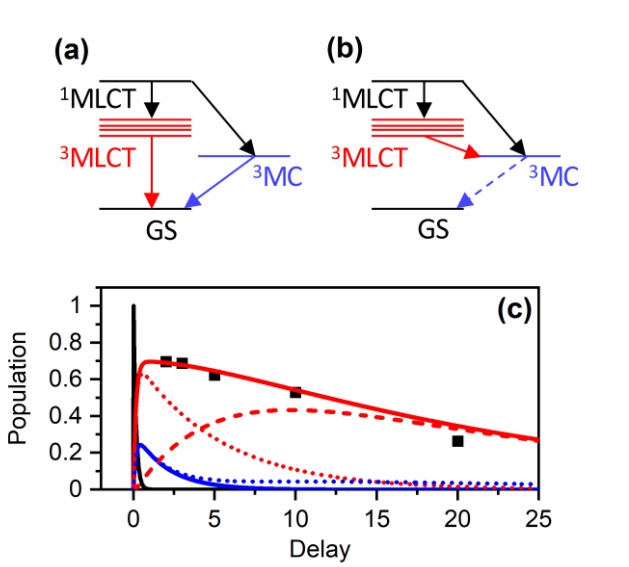

Figure 4 Models discussed for the photophysics of $[Fe(bmipc)_2]^{2+}$, with (a) parallel and (b) sequential ^{3}MLCT and ^{3}MC decay. (c) shows the corresponding population dynamics of the ^{1}MLCT (black, 220 fs) "hot" (red dotted line, 5.3 ps), "cold" (red dashed line, 19.9 ps) and sum of ^{3}MLCT (red solid line). The ^{3}MC state for the parallel (blue solid line) and sequential model (blue dotted line) is simulated with a lifetime of 2 ps in both cases. The FFT-Amplitudes at 140 cm^{-1} of the Pump-IVS experiments (black squares) are normalized for comparison with the ^{3}MLCT population. An initial branching ratio of 70%/30% ^{3}MLCT/^{3}MC was assumed.

In conclusion, by combining time-resolved vibrational coherence spectroscopy and quantum chemical calculations we investigated the photophysics of $[Fe(bmipc)_2]^{2+}$, a promising dye-sensitizer for solar energy conversion. Our work focuses on the highly debated spectrally elusive ^{3}MC states role in MLCT loss channels. Our results give very strong evidence that it drains population from the desirable MLCT manifold via an ultrafast branching of the initially populated ^{1}MLCT. Even with little to no excess photon energy the ^{3}MC state is populated impulsively. The resulting characteristic coherent breathing vibrations are observed via impulsive vibrational spectroscopy, establishing it as a lab-based method for identifying the excited state nature of transition metal complexes. Our findings imply, that the ISC to the longer lived

^{3}MLCT is rendered incomplete, fundamentally limiting charge injection processes slower than the ^{1}MLCT lifetime.

Experimental and Computational Section

$[Fe(bmipc)_2]^{2+}$ was prepared as described in the literature.[29] The samples were dissolved in acetonitrile. The optical densities of all samples were between 0.4 and 0.5 OD at their ground state absorption maximum in a 0.5 mm flow-cell cuvette. The experimental setups used for TA and (P-)IVS have been described elsewhere.[30] In the TA measurement, the pump pulse energy was set to 100 nJ. In (Pump-)IVS measurements the actinic pump pulse energy was set to 300 nJ, the push pulse energy to 100 nJ and the probe pulse energy to 20 nJ with spot diameters of 100 µm, 80 µm and 60 µm, respectively. The FWHM of IRF was about 55 fs and 35 fs in TA and IVS experiments, respectively.

$[Fe(bmipc)_2]^{2+}$ was optimised in the ground state and ^{3}MC and ^{3}MLCT states using DFT within the approximation of B3LYP* exchange and correlation functional and a def2-SVP basis set as implemented within the ORCA quantum chemistry package.[31, 32] While this is only valid for the lowest state of each multiplicity, both the ^{3}MC and ^{3}MLCT are the lowest triplets at their respective optimised geometries (Figure S8). Numerical frequencies calculations were carried out on the geometries optimised to ensure no negative frequencies.

Acknowledgements

This research was funded by the French Agence Nationale de la Recherche (ANR-16-CE07-0013-02). This work of the Interdisciplinary Thematic Institute QMat, as part of the ITI 2021-28 program of the University of Strasbourg, CNRS and Inserm,

was supported by IdEx Unistra (ANR 10 IDEX 0002), by SFRI STRAT'US project (ANR 20 SFRI 0012) and EUR QMAT ANR-17-EURE-0024 under the framework of the French Investments for the Future Program.

References

1. Lindh, L.; Chábera, P.; Rosemann, N. W.; Uhlig, J.; Wärnmark, K.; Yartsev, A.; Sundström, V.; Persson, P., Photophysics and Photochemistry of Iron Carbene Complexes for Solar Energy Conversion and Photocatalysis. *Catalysts* **2020,** *10* (3), Art. No. 315.
2. Wenger, O. S., Is Iron the New Ruthenium? *Chemistry – A European Journal* **2019,** *25* (24), 6043-6052.
3. Wenger, O. S., A bright future for photosensitizers. *Nature Chemistry* **2020,** *12* (4), 323-324.
4. Treiling, S.; Wang, C.; Förster, C.; Reichenauer, F.; Kalmbach, J.; Boden, P.; Harris, J. P.; Carrella, L. M.; Rentschler, E.; Resch-Genger, U.; Reber, C.; Seitz, M.; Gerhards, M.; Heinze, K., Luminescence and Light-Driven Energy and Electron Transfer from an Exceptionally Long-Lived Excited State of a Non-Innocent Chromium(III) Complex. *Angewandte Chemie International Edition* **2019,** *58* (50), 18075-18085.
5. Reddy Marri, A.; Marchini, E.; Cabanes, V. D.; Argazzi, R.; Pastore, M.; Caramori, S.; Gros, P. C., Record power conversion efficiencies for iron(ii)-NHC-sensitized DSSCs from rational molecular engineering and electrolyte optimization. *Journal of Materials Chemistry A* **2021**, 3540-3554.
6. Ferrere, S.; Gregg, B. A., Photosensitization of TiO2by [FeII(2,2'-bipyridine-4,4'-dicarboxylic acid)2(CN)2]: Band Selective Electron Injection from Ultra-Short-Lived Excited States. *Journal of the American Chemical Society* **1998,** *120* (4), 843-844.
7. McCusker, J. K., Electronic structure in the transition metal block and its implications for light harvesting. *Science* **2019,** *363* (6426), 484-488.
8. Monat, J. E.; McCusker, J. K., Femtosecond Excited-State Dynamics of an Iron(II) Polypyridyl Solar Cell Sensitizer Model. *Journal of the American Chemical Society* **2000,** *122* (17), 4092-4097.
9. Smeigh, A. L.; Creelman, M.; Mathies, R. A.; McCusker, J. K., Femtosecond Time-Resolved Optical and Raman Spectroscopy of Photoinduced Spin Crossover: Temporal Resolution of Low-to-High Spin Optical Switching. *Journal of the American Chemical Society* **2008,** *130* (43), 14105-14107.
10. Auböck, G.; Chergui, M., Sub-50-fs photoinduced spin crossover in [Fe(bpy)3]2+. *Nature Chemistry* **2015,** *7* (8), 629-633.
11. Cammarata, M.; Bertoni, R.; Lorenc, M.; Cailleau, H.; Di Matteo, S.; Mauriac, C.; Matar, S. F.; Lemke, H.; Chollet, M.; Ravy, S.; Laulhé, C.; Létard, J.-F.; Collet, E., Sequential Activation of Molecular Breathing and Bending during Spin-Crossover Photoswitching Revealed by Femtosecond Optical and X-Ray Absorption Spectroscopy. *Physical Review Letters* **2014,** *113* (22), Art. No. 227402.
12. Harlang, T. C. B.; Liu, Y.; Gordivska, O.; Fredin, L. A.; Ponseca, C. S.; Huang, P.; Chábera, P.; Kjaer, K. S.; Mateos, H.; Uhlig, J.; Lomoth, R.; Wallenberg, R.; Styring, S.; Persson, P.; Sundström, V.; Wärnmark, K., Iron sensitizer converts light to electrons with 92% yield. *Nature Chemistry* **2015,** *7* (11), 883-889.
13. Zimmer, P.; Müller, P.; Burkhardt, L.; Schepper, R.; Neuba, A.; Steube, J.; Dietrich, F.; Flörke, U.; Mangold, S.; Gerhards, M.; Bauer, M., N-Heterocyclic Carbene Complexes of Iron as Photosensitizers for Light-Induced Water Reduction. *European Journal of Inorganic Chemistry* **2017,** *2017* (11), 1504-1509.

14. Chábera, P.; Kjaer, K. S.; Prakash, O.; Honarfar, A.; Liu, Y.; Fredin, L. A.; Harlang, T. C. B.; Lidin, S.; Uhlig, J.; Sundström, V.; Lomoth, R.; Persson, P.; Wärnmark, K., FeII Hexa N-Heterocyclic Carbene Complex with a 528 ps Metal-to-Ligand Charge-Transfer Excited-State Lifetime. *The Journal of Physical Chemistry Letters* **2018,** *9* (3), 459-463.
15. Braun, J. D.; Lozada, I. B.; Kolodziej, C.; Burda, C.; Newman, K. M. E.; van Lierop, J.; Davis, R. L.; Herbert, D. E., Iron(ii) coordination complexes with panchromatic absorption and nanosecond charge-transfer excited state lifetimes. *Nature Chemistry* **2019,** *11* (12), 1144-1150.
16. Kjær, K. S.; Kaul, N.; Prakash, O.; Chábera, P.; Rosemann, N. W.; Honarfar, A.; Gordivska, O.; Fredin, L. A.; Bergquist, K.-E.; Häggström, L.; Ericsson, T.; Lindh, L.; Yartsev, A.; Styring, S.; Huang, P.; Uhlig, J.; Bendix, J.; Strand, D.; Sundström, V.; Persson, P.; Lomoth, R.; Wärnmark, K., Luminescence and reactivity of a charge-transfer excited iron complex with nanosecond lifetime. *Science* **2019,** *363* (6424), 249-253.
17. Magra, K.; Domenichini, E.; Francés-Monerris, A.; Cebrián, C.; Beley, M.; Darari, M.; Pastore, M.; Monari, A.; Assfeld, X.; Haacke, S.; Gros, P. C., Impact of thefac/merIsomerism on the Excited-State Dynamics of Pyridyl-carbene Fe(II) Complexes. *Inorganic Chemistry* **2019,** *58* (8), 5069-5081.
18. Magra, K.; Darari, M.; Domenichini, E.; Francés-Monerris, A.; Cebrián, C.; Beley, M.; Pastore, M.; Monari, A.; Assfeld, X.; Haacke, S.; Gros, P. C., Photophysical Investigation of Iron(II) Complexes Bearing Bidentate Annulated Isomeric Pyridine-NHC Ligands. *The Journal of Physical Chemistry C* **2020,** *124* (34), 18379-18389.
19. Kunnus, K.; Vacher, M.; Harlang, T. C. B.; Kjaer, K. S.; Haldrup, K.; Biasin, E.; van Driel, T. B.; Papai, M.; Chabera, P.; Liu, Y. Z.; Tatsuno, H.; Timm, C.; Kallman, E.; Delcey, M.; Hartsock, R. W.; Reinhard, M. E.; Koroidov, S.; Laursen, M. G.; Hansen, F. B.; Vester, P.; Christensen, M.; Sandberg, L.; Nemeth, Z.; Szemes, D. S.; Bajnoczi, E.; Alonso-Mori, R.; Glownia, J. M.; Nelson, S.; Sikorski, M.; Sokaras, D.; Lemke, H. T.; Canton, S.; Moller, K. B.; Nielsen, M. M.; Vank, G.; Warnmark, K.; Sundstrom, V.; Persson, P.; Lundberg, M.; Uhlig, J.; Gaffney, K. J., Vibrational wavepacket dynamics in Fe carbene photosensitizer determined with femtosecond X-ray emission and scattering. *Nat Commun* **2020,** *11* (1), Art. No. 634.
20. Paulus, B. C.; Adelman, S. L.; Jamula, L. L.; McCusker, J. K., Leveraging excited-state coherence for synthetic control of ultrafast dynamics. *Nature* **2020,** *582* (7811), 214-218.
21. Brown, A. M.; McCusker, C. E.; McCusker, J. K., Spectroelectrochemical identification of charge-transfer excited states in transition metal-based polypyridyl complexes. *Dalton Trans.* **2014,** *43* (47), 17635-17646.
22. Liu, L.; Duchanois, T.; Etienne, T.; Monari, A.; Beley, M.; Assfeld, X.; Haacke, S.; Gros, P. C., A new record excited state (MLCT)-M-3 lifetime for metalorganic iron(II) complexes. *Phys Chem Chem Phys* **2016,** *18* (18), 12550-12556.
23. Buckup, T.; Leonard, J., Multidimensional Vibrational Coherence Spectroscopy. *Topics Curr Chem* **2018,** *376* (5), Art. No. 35.
24. Papai, M.; Vanko, G.; Rozgony, T.; Penfold, T. J., High-Efficiency Iron Photosensitizer Explained with Quantum Wavepacket Dynamics. *J Phys Chem Lett* **2016,** *7* (11), 2009-2014.
25. Fredin, L. A.; Papai, M.; Rozsalyi, E.; Vanko, G.; Warnmark, K.; Sundstrom, V.; Persson, P., Exceptional Excited-State Lifetime of an Iron(II)-N-Heterocyclic Carbene Complex Explained. *J Phys Chem Lett* **2014,** *5* (12), 2066-2071.
26. Liu, L.; Agathangelou, D.; Roland, T.; Crégut, O.; Duchanois, T.; Beley, M.; Léonard, J.; Gros, P.; Haacke, S., High sensitivity fluorescence up-conversion spectroscopy of 3MLCT emission of metal-organic complexes. *EPJ Web Conf.* **2019,** *205*, Art. No. 09009.
27. Liu, Y. Z.; Harlang, T.; Canton, S. E.; Chabera, P.; Suarez-Alcantara, K.; Fleckhaus, A.; Vithanage, D. A.; Goransson, E.; Corani, A.; Lomoth, R.; Sundstrom, V.; Warnmark, K., Towards longer-lived metal-to-ligand charge transfer states of iron(II) complexes: an N-heterocyclic carbene approach. *Chem Commun* **2013,** *49* (57), 6412-6414.

28. Tatsuno, H.; Kjaer, K. S.; Kunnus, K.; Harlang, T. C. B.; Timm, C.; Guo, M. Y.; Chabera, P.; Fredin, L. A.; Hartsock, R. W.; Reinhard, M. E.; Koroidov, S.; Li, L.; Cordones, A. A.; Gordivska, O.; Prakash, O.; Liu, Y. Z.; Laursen, M. G.; Biasin, E.; Hansen, F. B.; Vester, P.; Christensen, M.; Haldrup, K.; Nemeth, Z.; Szemes, D. S.; Bajnoczi, E.; Vanko, G.; Van Driel, T. B.; Alonso-Mori, R.; Glownia, J. M.; Nelson, S.; Sikorski, M.; Lemke, H. T.; Sokaras, D.; Canton, S. E.; Dohn, A. O.; Moller, K. B.; Nielsen, M. M.; Gaffney, K. J.; Warnmark, K.; Sundstrom, V.; Persson, P.; Uhlig, J., Hot Branching Dynamics in a Light-Harvesting Iron Carbene Complex Revealed by Ultrafast X-ray Emission Spectroscopy. *Angew Chem Int Edit* **2020,** *59* (1), 364-372.
29. Duchanois, T.; Etienne, T.; Cebrian, C.; Liu, L.; Monari, A.; Beley, M.; Assfeld, X.; Haacke, S.; Gros, P. C., An Iron-Based Photosensitizer with Extended Excited-State Lifetime: Photophysical and Photovoltaic Properties. *European Journal of Inorganic Chemistry* **2015,** (14), 2469-2477.
30. Roy, P. P.; Kato, Y.; Abe-Yoshizumi, R.; Pieri, E.; Ferre, N.; Kandori, H.; Buckup, T., Mapping the ultrafast vibrational dynamics of all-trans and 13-cis retinal isomerization in Anabaena Sensory Rhodopsin. *Phys Chem Chem Phys* **2018,** *20* (48), 30159-30173.
31. Reiher, M.; Salomon, O.; Artur Hess, B., Reparameterization of hybrid functionals based on energy differences of states of different multiplicity. *Theoretical Chemistry Accounts: Theory, Computation, and Modeling (Theoretica Chimica Acta)* **2001,** *107* (1), 48-55.
32. Weigend, F., Accurate Coulomb-fitting basis sets for H to Rn. *Phys Chem Chem Phys* **2006,** *8* (9), 1057-1065.